TURBULENT DRAG REDUCTION CURVES FOR ANISOTROPIC PERMEABLE SUBSTRATES – ANALYSIS AND DIRECT NUMERICAL SIMULATIONS

Garazi Gómez-de-Segura
Department of Engineering
University of Cambridge
Trumpington St. CB2 1PZ, UK
gg406@cam.ac.uk

Ricardo García-Mayoral
Department of Engineering
University of Cambridge
Trumpington St. CB2 1PZ, UK
r.gmayoral@eng.cam.ac.uk

ABSTRACT

We explore the ability of a novel passive technology – anisotropic permeable substrates – to reduce turbulent skin-friction. We perform direct numerical simulations (DNSs) of channel flows bounded by permeable substrates, where the flow within the permeable medium is modelled using Brinkman's equation. The DNS results confirm theoretical predictions, and the obtained drag reduction curves are similar to those observed for riblets. For small permeabilities, the performance is linear with the difference between the streamwise and spanwise permeability lengthscales. This linear drag reduction regime breaks down for a critical value of the wall-normal permeability, beyond which the performance begins to degrade. We observe that the degradation is due to the formation of spanwise-coherent structures, associated to a Kelvin–Helmholtz-like instability of the mean flow. With the substrate configurations under study, the drag reduction can be as large as $\approx 20-25\%$ at a friction Reynolds number $\mathrm{Re}_\tau = 180$.

INTRODUCTION

The high skin friction experienced in turbulent flows represents a problem for several engineering applications. In this study, we present the potential of anisotropic permeable substrates to reduce turbulent skin friction, as recently proposed by Abderrahaman-Elena & García-Mayoral (2017).

Assuming that the shift of the logarithmic mean velocity profile with respect to a smooth-wall flow, ΔU^+, is Reynolds-number independent (Spalart & McLean, 2011; García-Mayoral *et al.*, 2019), the drag reduction or relative decrease of the friction coefficient is

$$\mathrm{DR} = 1 - 1 / \left(1 + \Delta U^+ / U_{\delta 0}^+\right)^2, \tag{1}$$

where $U_{\delta 0}$ is the free-stream velocity for a smooth-wall flow and depends on the friction Reynolds number Re_τ. Throughout the paper, we give results for drag reduction in terms of ΔU^+, so that they are Re_τ-independent.

Previous studies have shown that streamwise-preferential complex surfaces can reduce drag in turbulent flows. This reduction has recently been reviewed in García-Mayoral *et al.* (2019) as a virtual-origin effect for vanishingly small surface textures. The reduction of drag is essentially caused by an offset between the positions of the virtual, equivalent smooth walls perceived by the mean flow and by the overlying turbulence, but turbulence remains otherwise smooth-wall-like (Luchini *et al.*, 1991; Jiménez, 1994; Luchini, 1996; Gómez-de-Segura *et al.*, 2018). ΔU^+ is then

$$\Delta U^+ \approx \ell_U^+ - \ell_T^+, \tag{2}$$

where ℓ_U^+ is the depth below the reference plane of the virtual origin perceived by the mean flow, and ℓ_T^+ the depth of that perceived by turbulence. Luchini (1996) suggested that the virtual origin for turbulence could be identified as the origin experienced by the quasi-streamwise vortices. If the cross flow induced by quasi-streamwise vortices is hindered more than the streamwise mean flow, the vortices are, compared to a smooth wall, 'pushed away' from the apparent smooth wall perceived by the mean flow. As a result, the local momentum flux decreases, and the drag is reduced.

Recently, Abderrahaman-Elena & García-Mayoral (2017) suggested that streamwise-preferential anisotropic permeable substrates could produce such an effect. They derived analytical expressions for the virtual origins based on a Darcy-Brinkman model for the flow within the permeable substrates,

$$\nabla p = -\nu \mathbf{K}^{-1} \mathbf{u} + \nu \nabla^2 \mathbf{u}, \tag{3}$$

where $\mathbf{u} = (u, v, w)$ is the velocity vector, ν is the viscosity and $\mathbf{K}$ is the permeability tensor, with components K_x, K_y and K_z along its principal directions. The Brinkman term, $\nu \nabla^2 \mathbf{u}$, accounts for diffusion effects on scales larger than those integrated through volume averaging into Darcy's term, $\nu \mathbf{K}^{-1} \mathbf{u}$. Abderrahaman-Elena & García-Mayoral (2017) solved equation (3) in response to an overlying homogeneous shear, obtaining

$$\ell_U^+ = \sqrt{K_x^+} \tanh\left(\frac{h^+}{\sqrt{K_x^+}}\right), \quad \ell_T^+ = \sqrt{K_z^+} \tanh\left(\frac{h^+}{\sqrt{K_z^+}}\right). \tag{4}$$

They concluded that the highest performance for a given anisotropic material would be achieved for sufficiently deep substrates, where $\ell_U^+ \approx \sqrt{K_x^+}$ and $\ell_T^+ \approx \sqrt{K_z^+}$. The linear
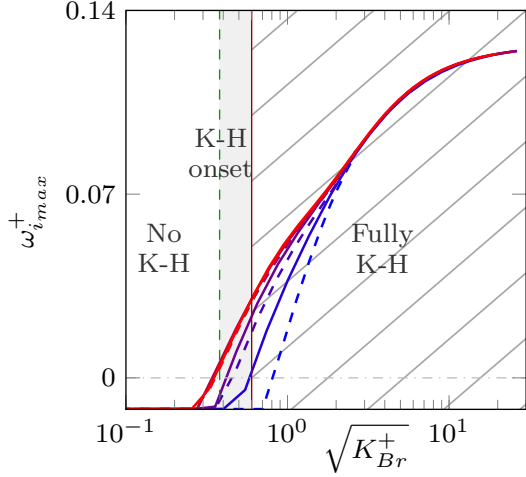
Figure 1. Amplification of the most unstable mode, $\omega_{i_{max}}^+$, as a function of the fitted permeability length $\sqrt{K_{Br}^+} \approx \sqrt{K_y^+}$ for various permeable substrates. $---$, $h^+ = 10$; ——, $h^+ = 100$; from blue to red, anisotropy ratios $K_x/K_y = 1, 10, 100, 1000$. The green and red lines define the thresholds for the degradation regime obtained from the DNS results: the green line corresponds to approximately the optimum ΔU^+ ($\sqrt{K_y^+} \approx 0.38$), and the red line corresponds to approximately the zero ΔU^+ line ($\sqrt{K_y^+} \approx 0.6$), after which drag increases.

regime of equation (2) would then be characterised by

$$\Delta U^+ \approx \sqrt{K_x^+} - \sqrt{K_z^+}. \quad (5)$$

To maximise drag reduction, we are thus interested in highly anisotropic materials with large K_x^+ and small K_z^+.

The linear regime of equations (2) and (5) is only valid as long as the surface texture is small compared to the near-wall turbulence structures. As the texture size increases, additional deleterious effects set in, degrading the drag-reducing behaviour and eventually leading to a drag increase. The development of Kelvin–Helmholtz rollers, which are ubiquitous over permeable substrates (Breugem *et al.*, 2006; Kuwata & Suga, 2016; Zampogna & Bottaro, 2016), have been proposed as a key drag-degrading mechanism (Abderrahaman-Elena & García-Mayoral, 2017; Gómez-de-Segura *et al.*, 2018). Based on a linear stability analysis, Gómez-de-Segura *et al.* (2018) estimated values for **K** at which Kelvin–Helmholtz instabilities would develop. For streamwise-preferential substrates, the instability is essentially governed by the wall-normal permeability, K_y^+. This is illustrated in figure 1, where the amplification of the most unstable mode for different substrates is captured by the parameter

$$K_{Br}^+ \approx K_y^+ \tanh(\sqrt{2K_x^+}/9) \tanh^2(h^+/\sqrt{12K_y^+}), \quad (6)$$

which in practical cases reduces to

$$K_{Br}^+ \approx K_y^+. \quad (7)$$

From figure 1, Gómez-de-Segura *et al.* (2018) defined a tentative threshold for the onset of drag-degrading rollers.

Using the DNS data, the threshold values were reassessed in Gómez-de Segura & García-Mayoral (2019) and set to $\sqrt{K_y^+} = 0.38 - 0.6$.

METHODOLOGY

We conduct DNSs in doubly-periodic channels of height 2δ delimited by two identical permeable substrates of thickness h. The DNS code, adapted from Fairhall & García-Mayoral (2018), solves the incompressible Navier-Stokes equations, with the density taken to be unity for simplicity. All simulations are conducted at a fixed friction Reynolds number $\mathrm{Re}_\tau = u_\tau \delta/\nu = 180$ by imposing a constant mean pressure gradient in $y \in [0, 2\delta]$. The kinematic viscosity is $\nu = 1/2870$ and we use a smooth-wall channel with the same mean pressure gradient as reference. The spatial discretisation is spectral in the wall-parallel directions x and z, with $2/3$ rule de-aliasing, and uses second-order centred finite differences on a staggered grid in the wall-normal direction. The computational domain is of size $2\pi \times \pi \times 2$ in the streamwise, spanwise and wall-normal directions, respectively. A grid with $192 \times 192 \times 153$ collocation points with grid stretching in y is used, which in viscous units gives a resolution of $\Delta x^+ \approx 5.9$, $\Delta z^+ \approx 2.9$, and $\Delta y^+ \simeq 0.3$ near the wall and $\Delta y^+ \simeq 3$ in the centre of the channel. For the temporal integration we use a fractional-step, Runge-Kutta discretisation, semi-implicit in the viscous terms and explicit in the advective terms. Once the statistically steady state had been reached, statistics for each simulation were obtained by averaging over approximately 100 eddy-turnovers.

The flow within the substrates was modelled using equation (3). The simplicity of this model allows for its analytical solution, which particularised at the substrate–channel interface gives

$$\hat{u}|_{y=0} = \mathscr{C}_{uu} \frac{d\hat{u}}{dy}\bigg|_{y=0} + \mathscr{C}_{uw} \frac{d\hat{w}}{dy}\bigg|_{y=0} + \mathscr{C}_{up}\hat{p}|_{y=0}, \quad (8a)$$

$$\hat{w}|_{y=0} = \mathscr{C}_{wu} \frac{d\hat{u}}{dy}\bigg|_{y=0} + \mathscr{C}_{ww} \frac{d\hat{w}}{dy}\bigg|_{y=0} + \mathscr{C}_{wp}\hat{p}|_{y=0}, \quad (8b)$$

$$\hat{v}|_{y=0} = \mathscr{C}_{vu} \frac{d\hat{u}}{dy}\bigg|_{y=0} + \mathscr{C}_{vw} \frac{d\hat{w}}{dy}\bigg|_{y=0} + \mathscr{C}_{vp}\hat{p}|_{y=0}. \quad (8c)$$

These are implemented as boundary conditions for the flow within the channel. In equation (8) the hat denotes variables in Fourier space. The coefficients $\mathscr{C}_{ij}$ depend on the structure of the permeable substrate through K_x, K_y, K_z and h, as well as on the overlying flow through the streamwise and spanwise wavenumbers, α_x and α_z.

RESULTS

As discussed above, the optimal substrate for drag reduction would seek to maximise the difference $\sqrt{K_x^+} - \sqrt{K_z^+}$ to obtain a large effective slip, while maintaining $\sqrt{K_y^+}$ as low as possible to inhibit the appearance of drag-increasing Kelvin–Helmholtz rollers. Since both K_y^+ and K_z^+ have a negative effect, we consider substrates with $K_x^+ > K_z^+ = K_y^+$.

We study three substrate configurations, characterised by three different anisotropy ratios $\phi_{xy} = \sqrt{K_x/K_y}$, with $\phi_{xy} \approx 3.5$, 5.5 and 11.5. For our main set of simulations,

Table 1. DNS parameters. $\sqrt{K_x^+}$, $\sqrt{K_y^+}$ and $\sqrt{K_z^+}$ are the streamwise, wall-normal and spanwise permeability lengths, h^+ is the thickness of the substrate, ΔU^+ is the shift of the velocity profile in the logarithmic region, and DR_{180} and DR_{5000} are the values of drag reduction for $Re_\tau = 180$ and $Re_\tau = 5000$, respectively, obtained using expression (1). The values DR_{5000} have been calculated using the reference smooth-wall data from Lee & Moser (2015). The first three substrate configurations A, B and C have thickness $h = 100\sqrt{K_y}$ and different anisotropy ratios ϕ_{xy}. The last three substrate configurations, C′, C″ and C‴, have $\phi_{xy} \approx 11.4$, as substrate C, but different thickness $h/\sqrt{K_x}$.

	Cases	$\sqrt{K_x^+}$	$\sqrt{K_y^+}$	$\sqrt{K_z^+}$	h^+	$U_b/U_{b_{sm}}$	ΔU^+	DR_{180}	DR_{5000}
Smooth		0	0	0	0	1.0	-	-	-
	A1	0.71	0.20	0.20	19.5	1.037	0.51	5.64	3.93
	A2	1.00	0.28	0.28	28.1	1.045	0.68	7.26	5.08
	A3	1.42	0.39	0.39	38.8	1.052	0.80	8.44	5.92
$\phi_{xy} = \sqrt{\frac{K_x}{K_y}} \approx 3.6$	A4	1.74	0.48	0.48	48.1	1.041	0.54	6.10	4.25
	A5	2.45	0.68	0.68	68.1	0.963	-0.68	-7.38	-4.99
	A6	3.61	1.00	1.00	100.2	0.819	-3.02	-42.31	-26.58
	A7	5.50	1.52	1.52	152.7	0.616	-6.59	-143.84	-76.46
	A8	10.97	3.04	3.04	304.2	0.381	-11.03	-546.15	-194.20
	B1	1.00	0.18	0.18	18.0	1.053	0.84	8.63	6.06
	B2	1.79	0.32	0.32	32.1	1.085	1.29	12.71	9.01
$\phi_{xy} = \sqrt{\frac{K_x}{K_y}} \approx 5.5$	B3	2.12	0.39	0.39	39.0	1.086	1.31	12.93	9.17
	B4	2.45	0.45	0.45	45.0	1.070	1.01	10.22	7.20
	B5	3.61	0.66	0.66	65.7	0.979	-0.46	-5.24	-3.56
	B6	5.48	1.00	1.00	100.0	0.792	-3.66	-56.35	-34.47
	B7	10.89	1.99	1.99	198.4	0.517	-8.66	-261.34	-120.00
	C1	1.00	0.09	0.09	9.0	1.062	0.98	9.89	6.96
	C2	1.73	0.15	0.15	14.0	1.106	1.67	16.01	11.45
	C3	2.45	0.21	0.21	22.0	1.145	2.24	20.63	14.93
$\phi_{xy} = \sqrt{\frac{K_x}{K_y}} \approx 11.4$	C4	3.6	0.32	0.32	32.0	1.178	2.84	25.10	18.38
	C5	4.48	0.39	0.39	39.1	1.183	2.87	25.34	18.56
	C6	5.47	0.48	0.48	47.9	1.152	2.34	21.38	15.50
	C7	10.89	0.96	0.96	95.6	0.898	-2.21	-29.35	-18.92
	C′1	2.45	0.21	0.21	3.67	1.130	2.00	18.74	13.49
$\frac{h}{\sqrt{K_x}} = 1.5$	C′2	3.61	0.32	0.32	5.40	1.171	2.70	24.12	17.62
	C′3	5.49	0.48	0.48	8.23	1.156	2.40	21.87	15.88
	C′4	10.84	0.95	0.95	16.26	0.962	-0.90	-10.84	-7.27
	C″1	3.61	0.32	0.32	3.61	1.154	2.42	22.02	15.99
	C″2	5.48	0.48	0.48	5.51	1.163	2.53	22.86	16.64
$\frac{h}{\sqrt{K_x}} = 1.0$	C″3	7.01	0.62	0.62	7.01	1.127	1.90	17.93	12.88
	C″4	9.03	0.79	0.79	9.03	1.066	0.84	8.62	6.05
	C″5	10.85	0.95	0.95	11.03	1.001	-0.12	-1.32	-0.91
	C‴1	2.45	0.21	0.21	1.22	1.063	0.93	9.46	6.65
	C‴2	3.62	0.32	0.32	1.86	1.091	1.36	13.35	9.48
$\frac{h}{\sqrt{K_x}} = 0.5$	C‴3	5.47	0.48	0.48	2.74	1.133	2.04	19.11	13.77
	C‴4	7.01	0.62	0.62	3.50	1.153	2.39	21.81	15.83
	C‴5	9.03	0.79	0.79	4.52	1.129	1.95	18.34	13.19
	C‴6	10.83	0.95	0.95	5.42	1.092	1.30	12.88	9.13

the substrates have thickness $h = 100\sqrt{K_y}$, large enough for the problem to become independent of h. An additional subset of simulations was conducted to explore the effect of a finite h on the substrate performance. For a given configuration, i.e. a fixed ϕ_{xy} and $h/\sqrt{K_y}$, we have conducted various simulations with increasing Reynolds number based on the texture size, $K_x^+ \in [0.5 - 117]$. The simulations are summarised in table 1.

The virtual-origin model in equations (2) and (5) is based on the idea that the near-wall cycle remains smooth-wall-like, other than by being displaced a depth ℓ_T towards the substrate. Given that the origin perceived by turbulence is expected to be at $y = -\ell_T \approx -\sqrt{K_z}$, throughout this section results are scaled taking that as the reference for the wall-normal height, with the friction velocity calculated at $y = -\sqrt{K_z}$.

The drag-reduction curves from the main set of DNSs are shown in figure 2. For small permeabilities, a linear drag-reduction regime is observed. The prediction $\Delta U^+ = \ell_U^+ - \ell_T^+ \approx \sqrt{K_x^+} - \sqrt{K_z^+}$ of equation (5) agrees well with the DNS results, and the three substrate configurations exhibit roughly the same initial reduced slope in figure 2(b). The breakdown of the linear regime of drag reduction, however, occurs for different values of $\sqrt{K_x^+} - \sqrt{K_z^+}$ depending on the substrate.

In contrast, when the lengthscale is represented in terms of $\sqrt{K_y^+}$, the parameter predicted to trigger the onset
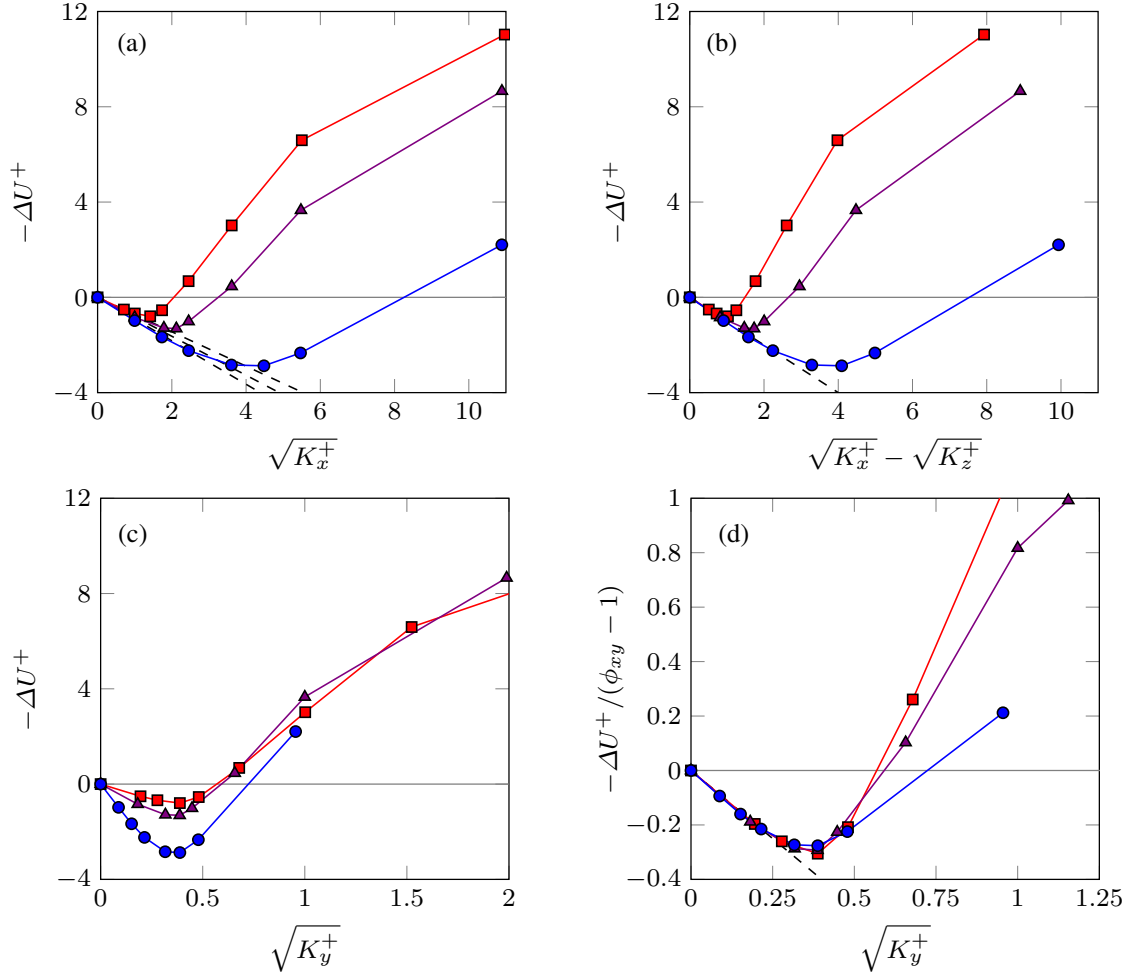
Figure 2. Drag reduction curves for substrates with different anisotropy ratios. —●—, $\phi_{xy} \approx 11.4$; —▲—, $\phi_{xy} \approx 5.5$; and —■—, $\phi_{xy} \approx 3.6$. The symbols correspond to DNSs listed in table 1. ΔU^+ is represented versus (a) the streamwise permeability lengthscale, $\sqrt{K_x^+}$; (b) its predicted value in the linear regime, $\sqrt{K_x^+} - \sqrt{K_z^+}$; (c) the wall-normal permeability lengthscale, $\sqrt{K_y^+}$. (d) ΔU^+, reduced with its predicted slope, versus the wall-normal permeability lengthscale, $\sqrt{K_y^+}$. – – –, theoretical prediction $\Delta U^+ = \sqrt{K_x^+} - \sqrt{K_z^+}$.
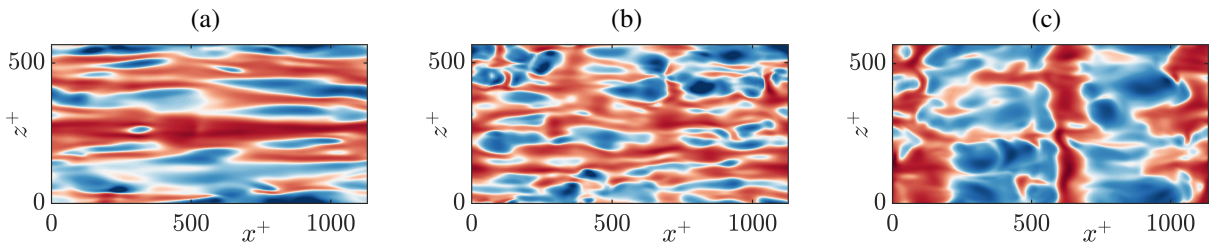
Figure 3. Instantaneous realisations of streamwise velocity at a plane parallel to the interface ($y^+ \approx 2-3$) for a given substrate configuration with $\phi_{xy} \approx 11.5$. From left to right K_x^+ increases: (a) $K_x^+ = 3$, which lies on the linear regime of the drag reduction curve; (b) $K_x^+ = 30$, which is beyond the breakdown; (c) $K_x^+ = 117$, which lies in the drag-increasing regime.

of Kelvin–Helmholtz-like rollers, the location of the breakdown coincides for all the curves, as shown in figure 2(c). For all substrate configurations, the drag reduction is maximum for $\sqrt{K_y^+} \approx 0.38$ and the drag becomes greater than for a smooth wall for $\sqrt{K_y^+} \gtrsim 0.6$.

The degradation of the performance is consistent with the appearance of spanwise-coherent rollers. To illustrate how the overlying turbulence is modified as $\sqrt{K_y^+}$ increases, figure 3 shows instantaneous realisations of u immediately above the substrate–channel interface. For $\sqrt{K_y^+} \gtrsim 0.6$, the drag-increasing rollers become prevalent in the flow, outweighing the drag-reducing effect of the streamwise slip and eventually leading to an increase of drag.

The common linear drag reduction behaviour, observed in figure 2(b), and its common breakdown, observed in figure 2(c), are condensed in figure 2(d). This is done by dividing ΔU^+ from figure 2(c) by the slope for each curve expected from equation (5) for $K_z^+ = K_y^+$, i.e. $\phi_{xy} - 1$. Given
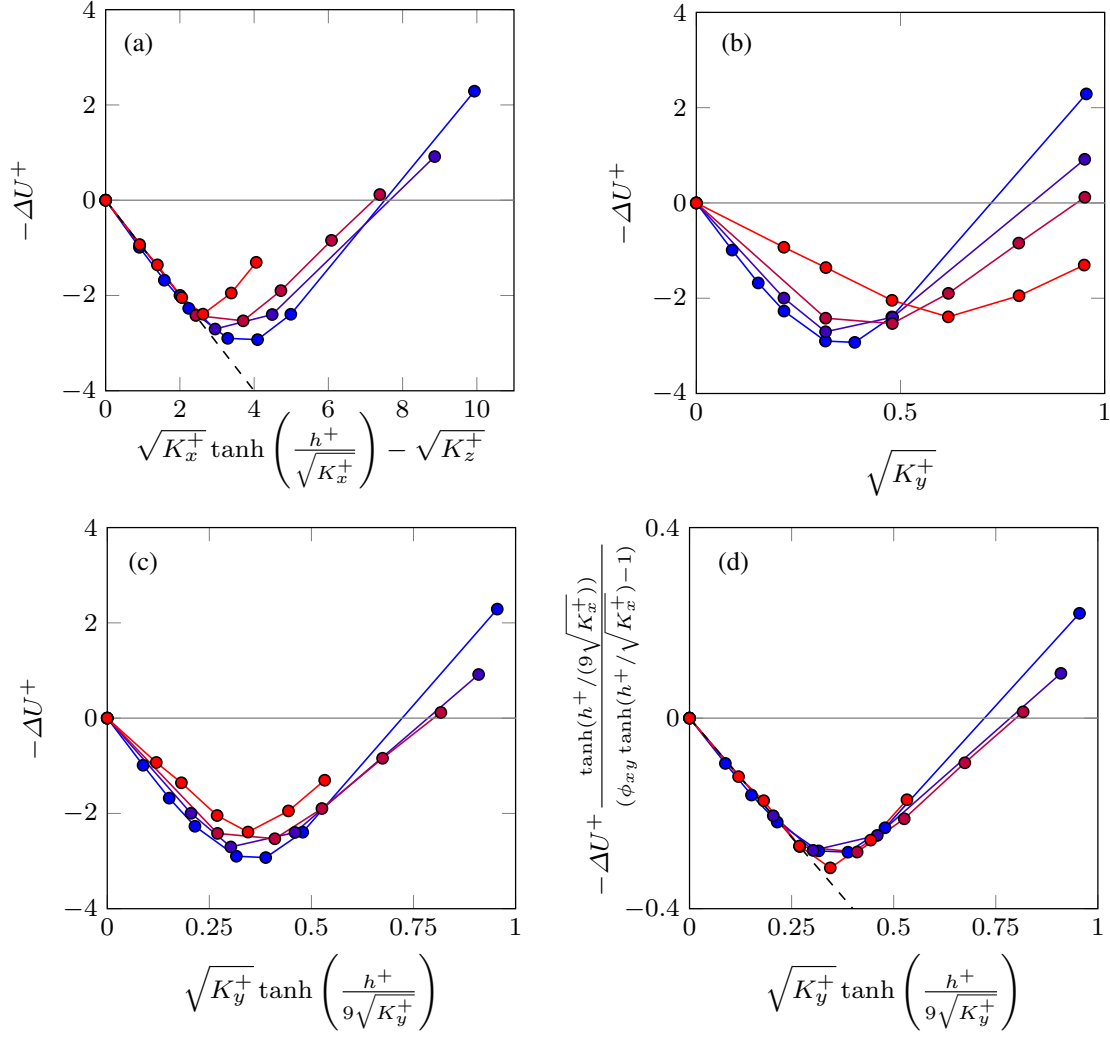
Figure 4. Drag reduction curves for substrates with the same permeabilities but different substrate thickness. From blue to red, representing decreasing thickness, cases C1-C7, C′1-C′7, C″1-C″7, and C‴1-C‴7, corresponding to $h/\sqrt{K_x} = 8.8$, 1.5, 1.0, and 0.5. ΔU^+ is represented versus (a) its theoretical value in the linear regime; (b) the wall-normal permeability lengthscale, $\sqrt{K_y^+}$; (c) the fitted permeability lengthscale for the breakdown $\sqrt{K_{Br}'^+}$. (d) ΔU^+, reduced with its predicted linear slope, versus $\sqrt{K_{Br}'^+}$. – – –, theoretical prediction $\Delta U^+ = \sqrt{K_x^+}\tanh(h^+/\sqrt{K_x^+}) - \sqrt{K_z^+}$.

that in this equation ΔU^+ depends only on ϕ_{xy} and $\sqrt{K_y^+}$, the general collapse suggested by this figure can be used to estimate the performance of permeable substrates different to those explored in this work. Considering that the maximum ΔU^+ in figure 2(d) occurs for $\sqrt{K_y^+}|_{opt} \approx 0.38$ and is approximately 80% of that estimated by equation (5), the maximum ΔU^+ would depend only on the anisotropy ratio,

$$\Delta U_{max}^+ \approx 0.8 \times 0.38 \times (\phi_{xy} - 1). \qquad (9)$$

For the substrate with the largest ϕ_{xy} considered here, $\phi_{xy} \approx 11.5$, the obtained ΔU^+ corresponds to DR $\approx 25\%$ at $\mathrm{Re}_\tau = 180$. For substrates with different cross permeabilities, $\phi_{zy} = \sqrt{K_z/K_y} \neq 1$, it follows from equation (5) that $\Delta U_{max}^+ \approx 0.8 \times 0.38 \times (\phi_{xy} - \phi_{zy})$.

The secondary set of simulations aims to explore the effect of the substrate depth on ΔU^+, and to test if the performance could be improved by reducing the depth enough for it to become a parameter in the problem. For this, the same substrate of cases C1-C7 is studied with depths

$h/\sqrt{K_x} = 1.5$, 1.0, and 0.5. From equations (4), we can expect shallower substrates to have smaller ℓ_U^+ and ℓ_T^+, as the hyperbolic tangent terms become smaller than unity. This would reduce the slope of the ΔU^+ curve in the linear regime and be an adverse effect. However, a reduced depth would also have the beneficial effect of making the substrate more robust to the onset of Kelvin–Helmholtz-like rollers, as at a given Reynolds number (i.e. $\sqrt{K_x^+}$, $\sqrt{K_y^+}$) equation (6) would predict a smaller $\sqrt{K_{Br}^+}$. Note also that $\sqrt{K_{Br}^+}$ is a parameter empirically fitted to the results from the linear stability model, and that the actual results show that shallower substrates have in fact a delayed Kelvin–Helmholtz onset in terms of $\sqrt{K_{Br}^+}$, as shown in figure 1.

The results for ΔU^+ for the shallow substrates of the secondary set of simulations are portrayed in figure 4, compared with the corresponding deep substrate from the main set, cases C1-C7. Given that all of our substrates are more permeable in x, the first terms to experience the effect of a finite h in equations (4) and (6) are those where h ap-

pears scaled with $\sqrt{K_x}$. Note that if we had considered values of h small enough for $h/\sqrt{K_z}$ to be also small, we would have $\ell_U^+ \approx \ell_T^+ \approx h^+$, which would yield no drag-reducing effect. For the values of $h/\sqrt{K_x}$ considered, we have $h/\sqrt{K_y} = h/\sqrt{K_z} = 6$, 11 and 17, so the corresponding hyperbolic tangent terms in equations (4) and (6) are still essentially unity. This can be appreciated, for instance, in figure 4(a), where the predicted slope in the linear regime has been adjusted for the effect of h^+ on the streamwise slip, $\ell_U^+ \approx \sqrt{K_x^+} \tanh(h^+/\sqrt{K_x^+})$, but the spanwise slip remains essentially $\ell_T^+ \approx \sqrt{K_z^+}$. Figure 4(b), however, shows that $\sqrt{K_y^+}$ is no longer adequate to parametrise the onset of the degradation. Panel (c), in turn, suggests that a suitable alternative is $\sqrt{K_{Br}'^+} = \sqrt{K_y^+} \tanh(h^+/(9\sqrt{K_y^+}))$, and that the optimum value is still $\sqrt{K_{Br}'^+} \approx 0.38$, as in figure 2. All the curves can be once more collapsed by reducing ΔU^+ with its predicted slope in the linear regime and expressing the Reynolds number in terms of $\sqrt{K_{Br}'^+}$, as is done in panel (d). This suggests that the optimum performance for shallow substrates can also be predicted and would be $\Delta U_{max}^+ \approx 0.8 \times 0.38 \times [\phi_{xy} \tanh(h/\sqrt{K_x}) - \phi_{zy}]/\tanh(h/9\sqrt{K_y})$. Note, however, that ΔU_{max}^+ decreases slightly as the substrate depth is reduced, as can be appreciated in panel (a), and that even if there is a delay in the critical $\sqrt{K_y^+}$ in absolute terms, as observed in panel (b), any gain in the relative width of the 'drag bucket' region – the near-optimal range – is insignificant, as is clear from panel (d).

CONCLUSIONS

We have explored the ability of streamwise-preferential permeable substrates to reduce turbulent skin friction through theoretical predictions and subsequent DNSs of channel flows. For sufficiently small surface textures, the drag reduction behaviour is linear with the difference $\sqrt{K_x^+} - \sqrt{K_z^+}$. The effect of the substrates is therefore reduced to a mere offset between the origins for the mean flow and turbulence (García-Mayoral *et al.*, 2019). As the texture size increases, we observe the formation of drag-increasing spanwise-coherent rollers, associated to a Kelvin–Helmholtz instability. These structures appear to disrupt the near-wall cycle and modify the near-wall turbulence, increasing the Reynolds stress and, consequently, the drag. The instability, and hence the breakdown, are found to be governed by the wall-normal permeability. In particular, the optimum ΔU^+ peaks at $\sqrt{K_y^+} \approx 0.38$ independently of the substrate configuration. For larger $\sqrt{K_y^+}$, these drag-increasing spanwise rollers become prevalent in the flow, outweighing the drag-reducing

effect of the streamwise slip and eventually leading to an increase of drag.

The understanding gained from the present DNSs and theoretical predictions can be used as a guideline to explore further the drag-reducing ability of these substrates. The present results suggest that such substrates may provide a performance substantially better than riblets.

REFERENCES

Abderrahaman-Elena, N. & García-Mayoral, R. 2017 Analysis of anisotropic permeable surfaces for turbulent drag reduction. *Phys. Rev. Fluids* **2**, 114609.

Breugem, W. P., Boersma, B. J. & Uittenbogaard, R. E. 2006 The influence of wall permeability on turbulent channel flow. *J. Fluid Mech.* **562**, 35–72.

Fairhall, C. T. & García-Mayoral, R. 2018 Spectral analysis of slip-length model for turbulence over textured superhydrophobic surfaces. *Flow Turb. Combust.* **100** (4), 961–978.

García-Mayoral, R., Gómez-de-Segura, G. & Fairhall, C. T. 2019 The control of near-wall turbulence through surface texturing. *Fluid Dyn. Res.* **51** (1).

Gómez-de-Segura, G., Sharma, A. & García-Mayoral, R. 2018 Turbulent drag reduction using anisotropic permeable substrates. *Flow Turb. Combust.* **100** (4), 995–1014.

Jiménez, J. 1994 On the structure and control of near wall turbulence. *Phys. Fluids* **6**, 944.

Kuwata, Y & Suga, K 2016 Lattice Boltzmann direct numerical simulation of interface turbulence over porous and rough walls. *Int. J. Heat Fluid Flow* **0**, 1–13.

Lee, M. & Moser, R. D. 2015 Direct numerical simulation of turbulent channel flow up to $Re_\tau = 5200$. *J. Fluid Mech.* **774** (1), 395–415.

Luchini, P. 1996 Reducing the turbulent skin friction. *Comput. Methods Appl. Sci. - Proc. 3rd ECCOMAS CFD Conf.* pp. 466–470.

Luchini, P., Manzo, F. & Pozzi, A. 1991 Resistance of a grooved surface to parallel flow and cross-flow. *J. Fluid Mech.* **228**, 87–109.

Gómez-de Segura, G. & García-Mayoral, R. 2019 Turbulent drag reduction by anisotropic permeable substrates – analysis and direct numerical simulations. *Submitted to J. Fluid Mech.* .

Spalart, P. R. & McLean, J. D. 2011 Drag reduction: enticing turbulence, and then an industry. *Phil. Trans. R. Soc. A* **369**, 1556–1569.

Zampogna, G. A. & Bottaro, A. 2016 Fluid flow over and through a regular bundle of rigid fibres. *J. Fluid Mech.* **792**, 5–35.